Ultraviolet micro-Raman spectroscopy stress mapping of a 75-mm GaN-on-diamond wafer

B. L. Hancock,[1] M. Nazari,[1] J. Anderson,[1] E. Piner,[1,2] F. Faili,[3] S. Oh,[3] D. Twitchen,[3] S. Graham,[4] and M. Holtz[1,2,a)]
[1]*Materials Science, Engineering, and Commercialization, Texas State University, San Marcos, Texas 78666, USA*
[2]*Department of Physics, Texas State University, San Marcos, Texas 78666, USA*
[3]*Element Six Technologies, U.S. Corporation, Santa Clara, California 95054, USA*
[4]*Woodruff School of Mechanical Engineering, Georgia Institute of Technology, Atlanta, Georgia 30332, USA*

(Received 15 March 2016; accepted 13 May 2016; published online 23 May 2016)

Full-wafer stress mapping is accomplished using visible and ultraviolet (UV) micro-Raman spectroscopy of a 730-nm thick GaN layer integrated with diamond grown by chemical vapor deposition. The UV measurements taken from both sides of the wafer reveal a higher tensile stress of 0.86 ± 0.07 GPa at the free GaN surface compared to 0.23 ± 0.06 GPa from the GaN/diamond interface, each with good cross-wafer uniformity. Factors influencing the overall stress and stress gradient are understood based on relaxation from dislocations in the GaN which vary in density along the growth direction. Simulations incorporating a model for stress relaxation in the GaN elastic modulus adequately describe the observed dependence. *Published by AIP Publishing.*
[http://dx.doi.org/10.1063/1.4952596]

Thermal management in electronics is currently the principle barrier to decreasing device size and increasing power densities. This is particularly the case in AlGaN/GaN high electron mobility transistors (HEMTs) where current flows within the <10-nm thick two-dimensional electron gas. The resulting self-heating produces localized temperature rises as high as 350 °C.[1] Efforts for improving heat extraction from the active region, such as incorporation of substrates with high thermal conductivity, have shown substantial promise for thermal management.[2,3]

Removing the growth substrate (e.g., Si) and integrating diamond as a heat spreader directly under the GaN layer for GaN-based devices is particularly attractive due to its high thermal conductivity (up to 2000 W/mK) when compared to traditional Si or 6H-SiC substrates.[4] Direct growth of diamond, using chemical vapor deposition (CVD), on device-quality GaN HEMT stacks has recently been demonstrated for wafer sizes up to 100 mm with diamond substrate thicknesses up to 100 μm.[2,5,6] As the scale-up processes for these wafers progress, investigations addressing the effects of growth methods on material quality are essential for future device development. The focus of this study is to examine mechanical stresses and stress gradients present in the GaN layer for device-quality GaN-on-diamond, including full wafers, to understand the causes for observed variations in the through-layer stress across the wafer.

Stresses in III-nitride films and heterostructures arise from lattice mismatch and differences in the coefficients of thermal expansion (CTE) between the diverse layers during high-temperature processing.[7] Subsequent processing and development steps, such as the deposition of adhesion/passivation layers (e.g., SiO_2, SiN_x), wafer bonding to sacrificial handle wafers, and the growth of CVD diamond also contribute additional stresses to the epitaxial layers. The effects of stress on the material quality and ultimate device performance have been investigated; concerns include layer cracking,[8] bow/warping,[9] and changes in the electrical behavior of HEMTs.[10,11]

Raman spectroscopy is a non-contact, non-destructive method which can be used for measuring stress in GaN layers. With micron lateral resolution, micro-Raman techniques are advantageous for spatial mapping of non-uniformities and material quality across fabricated wafers. Biaxial compressive (<0) and tensile (>0) stresses σ_{xx} in the GaN layer are readily observed through blue and red shifts in the Raman-active E_2^2-symmetry phonon, respectively.[7,9,12] The majority of micro-Raman investigations have been carried out using excitation in the visible wavelength range. Because GaN is transparent to visible light, these studies provide an average of the stresses throughout either the thickness of the GaN layer or within the beam waist of the focusing objective for thick materials.

In contrast, the optical penetration depth (d_{opt}) of the 363.8-nm near-ultraviolet (UV) excitation used here is approximately 100–130 nm in GaN. This value is obtained based on the optical attenuation coefficient rendered from complex dielectric function spectra of thick GaN,[13] and rigidly shifting the dependence to account for the effects of tensile stress. The proximity of the laser photon energy to the abruptly changing absorption edge makes d_{opt} sensitive to stress. The same approach for relaxed GaN results in an estimate of $d_{opt} < 150$ nm. Performing measurements at this wavelength from each side of the finished wafer allows stress determination in the GaN near the AlGaN/GaN surface (denoted *GaN side*) and through the transparent diamond layer to interrogate the GaN at this interface (denoted *GaN/D side*). These studies are used to produce a map through coordinated measurements on a 10-mm grid from each side of the wafer with <0.5-mm positioning precision, as illustrated in Fig. 1(a). By combining the UV results with visible (514.5 nm) micro-Raman measurements, we obtain, respectively, a stress map of the GaN and GaN/D sides and of

a)Mark.Holtz@txstate.edu

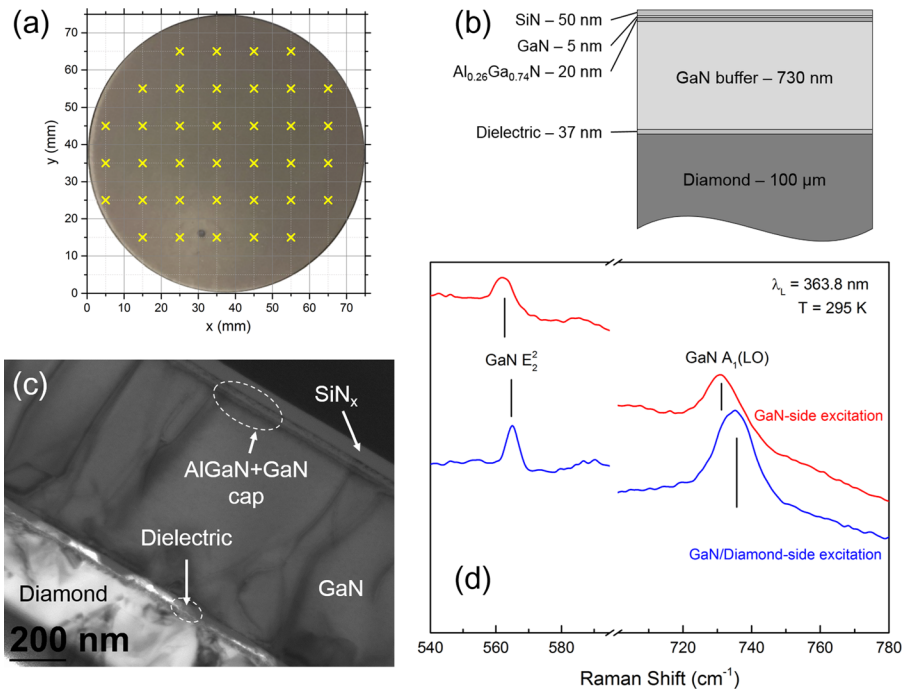

FIG. 1. (a) Coordinate system used for micro-Raman stress mapping with "x" denoting measurement positions across the wafer. (b) Wafer material stack with thicknesses for the GaN-on-diamond wafer studied. GaN layer thickness varies <3% across the full wafer based on the standard deviation. (c) TEM image of the GaN-on-diamond cross-section. (d) Representative UV micro-Raman spectra.

average stress through the layer. Details of the UV micro-Raman apparatus have been previously described.[1]

The 75-mm wafer investigated consists of a CVD diamond substrate grown on AlGaN/GaN HEMT device layers grown separately by metalorganic CVD. The material stack is illustrated in Fig. 1(b). The GaN-on-diamond fabrication has been previously described.[14] Briefly, the GaN-side of the AlGaN/GaN-on-Si wafer is bonded to a sacrificial handle wafer. The silicon substrate and transition layers are then removed and a dielectric layer deposited on the exposed GaN to facilitate diamond seeding. The thick ($\sim$100 μm) polycrystalline diamond is grown via microwave-enhanced CVD. The handle wafer is then removed, resulting in a standalone GaN-on-diamond wafer. A representative cross-section, obtained using transmission electron microscopy (TEM) and to be discussed in more detail later, is shown in Fig. 1(c).

Typical UV micro-Raman spectra in Fig. 1(d), obtained from the GaN- and GaN/D-sides of the wafer, show the allowed E_2^2 and A_1(LO) phonons. The broad background originates from photoluminescence (PL) from the GaN. Incident excitation power at the sample surface was $\sim$32 μW. When focused to a $\sim$3 μm diameter spot, the corresponding power density is within the range of negligible laser heating.[1] Peak positions ω are determined by fitting Lorentzian functions to the data with typical uncertainty $\pm 0.1\,\mathrm{cm}^{-1}$. Shifts from the un-strained phonon position, $\omega - \omega_0$, are used to determine biaxial stress values

$$\sigma_{xx} = (\omega - \omega_0)/k_R, \tag{1}$$

where k_R is the Raman stress factor. For the E_2^2 phonon, we use $k_R^{E_2^2} = -3.4 \pm 0.3\,\mathrm{cm}^{-1}/\mathrm{GPa}$ (Refs. 9 and 12) and $\omega_0 = 567.3 \pm 0.1\,\mathrm{cm}^{-1}$ measured from a strain-relaxed 55-μm GaN film. Uncertainty in the stress originates from the peak energies and k_R.

Figure 2(a) shows the map of E_2^2 phonon energy from the UV micro-Raman measurements from the GaN and GaN/D sides of the wafer. A red shift from ω_0 is observed in both cases. Moreover, a significant difference is observed in values obtained from the two sides of the GaN. The right-hand axis shows calculated stress from the E_2^2 peak position using Eq. (1). The resulting map reveals a significant

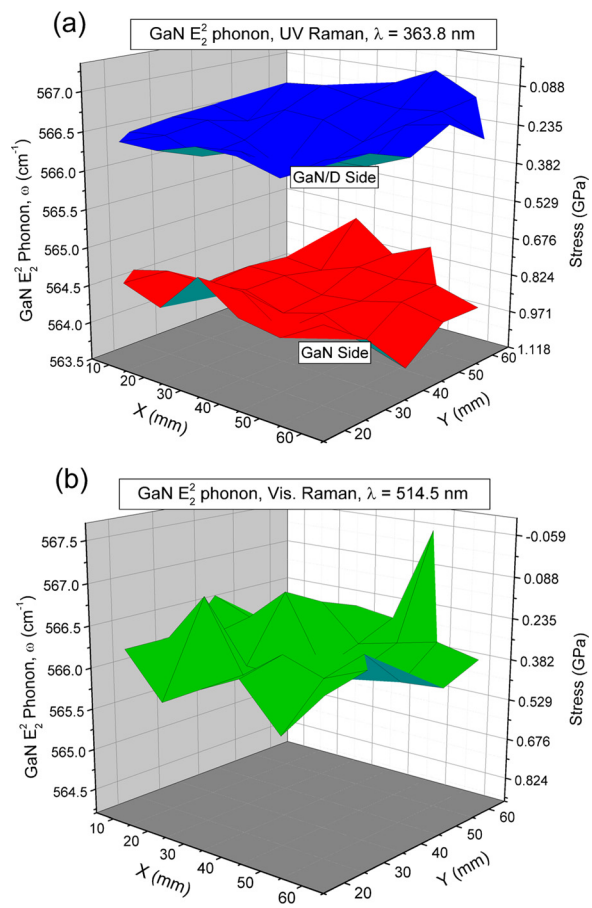

FIG. 2. (a) Map of E_2^2 phonon energy from micro-Raman measurements for (a) UV excitation and (b) visible excitation. The upper (lower) surface manifold in (a) corresponds to the measurement from the GaN/D (GaN) side of the wafer. The right-hand axis in both graphs shows the calculated stresses for each measurement.

gradient in the tensile stresses between the top and bottom interfaces of the GaN layer. The GaN-side tensile stress ranges from 0.67 to 1.0 GPa, with average value 0.86 GPa. For the GaN/D side, the tensile stress ranges from 0.075 to 0.37 GPa with average value 0.23 GPa. Typical uncertainties for the individual data points are ±0.09 and 0.05 GPa for measurements from the GaN and GaN/D sides, respectively. The corresponding standard deviations in the mean stresses from the two manifolds are 0.07 and 0.06 GPa. As mentioned above, a large stress gradient is not expected for a uniform thin film. PL measurements, to be reported separately, confirm the presence of the stress gradient.

The peak position map from visible micro-Raman measurements of the E_2^2 phonon is shown in Fig. 2(b), along with the corresponding stress values on the right-hand axis. The tensile stress from these measurements ranges from 0.12 to 0.44 GPa, plus one point at −0.04 GPa. An average tensile stress of $\sigma_{ave} = 0.32$ GPa was obtained across the wafer with uncertainty values of individual data points ±0.06 GPa and standard deviation of 0.10 GPa from this map. At this laser wavelength, the measurement represents a volume-(thickness-) weighted average stress throughout the 730-nm thick GaN layer. This is in contrast with the UV measurements, which provide stress values within the first 100–130 nm for the GaN and GaN/D sides.

Processing of the GaN-on-diamond wafer involves multiple high-temperature steps[5] which may contribute to thermal strain between adjacent layers. Biaxial thermal stress, σ_{xx}, due to CTE differences between a deposited film (thickness d_f) and substrate (thickness d_s) can be described by Stoney's equation[15]

$$\sigma_{xx} = \frac{\int_{T_0}^{T}\left[\alpha_s(T') - \alpha_f(T')\right]dT'}{\left\{\left[(1-\nu_f)/d_f E_f\right] + \left[(1-\nu_s)/d_s E_s\right]\right\} d_f} \rightarrow \frac{E_f}{1-\nu_f}\int_{T_0}^{T}\left[\alpha_s(T') - \alpha_f(T')\right]dT', \quad (2)$$

where for the substrate (film) $E_{s(f)}$ is the Young's modulus, $\alpha_{s(f)}$ is the temperature-dependent CTE value, $\nu_{s(f)}$ is the corresponding Poisson ratio,[9,16] and T_0 (T) is the initial (final) temperature. The limiting case is valid when $d_f \ll d_s$, as we have here. To describe stress in our multi-layered scenario, we carried out finite element (FE) simulations.[17] Because cooling in the fabrication steps covers large ranges in temperature, temperature-dependent CTE values were employed for each material in the simulations, using values along the *a*-axis for $\alpha_{GaN}(T)$.[16,18–21]

Simulations of a uniform GaN layer after high-T processing result in uniform thermal stress, as expected. The counterintuitive stress gradient, obtained via UV micro-Raman, suggests a variation in the GaN material properties may be responsible for the gradient. One plausible candidate is the ubiquitous presence of threading dislocations (TDs) in the GaN. TD densities are known to vary considerably along the growth direction in GaN.[22,23] It has been previously shown that *global* relaxation of biaxial strain in GaN is attributable to *local* relaxation near threading dislocations.[9] Assuming strain is relaxed in the immediate proximity of a TD, with characteristic length L, an average relaxation factor may be supposed

$$f = nL^2, \quad (3)$$

where n represents the TD area density. The resulting mixture of "ideal" GaN interspersed with microscopic, relaxed regions has an effective elastic modulus

$$E_{GaN}^{eff} = (1-f)E_{GaN}^{bulk}, \quad (4)$$

where E_{GaN}^{bulk} represents the *un-strained* elastic modulus for the material.[24] For GaN, we use $E_{GaN}^{bulk} = 324$ GPa and $\nu = 0.20 \pm 0.02$.[7,9] The relaxation effects of Eq. (4) were incorporated into the simulations using f as a fit parameter for the GaN and GaN/D regions of the layer. Because we have two stress values from the UV (σ_{GaN} and $\sigma_{GaN/D}$) plus the average stress (σ_{ave}) from visible micro-Raman measurements, we adopt a simple model comprised of two regions with different relaxation factors and thicknesses denoted t_1 and t_2. This is reasonable for MOCVD-grown GaN in which the final (device) regime (thickness t_1) is typically less defective than the initial growth stages (t_2) adjacent to the transition layers.[25] Our model consists of three parameters (f_{GaN}, $f_{GaN/D}$, and t_1 or t_2, where $t_1 + t_2 = t = 730$ nm) which are determined based on the three measured stress values. We estimate t_1 using

$$\sigma_{ave} = \left(t_1\sigma_{GaN} + t_2\sigma_{GaN/D}\right)/\left(t_1 + t_2\right). \quad (5)$$

From this, we determine $t_1 = 100 \pm 10$ nm and $t_2 = 630 \pm 90$ nm. Using these values, and incorporating Young's modulus from Eq. (4), the stress cross-section may be simulated to determine the remaining unknown relaxation factors f_{GaN} and $f_{GaN/D}$.

The step-by-step wafer fabrication was simulated to recreate the effects of thermal expansion at each major stage of the process upon cooling to room temperature: nitride MOCVD growth (~1100 °C), wafer bonding (~700 °C), and diamond CVD growth (~800 °C). Because the thicker layers play the dominant role in the overall thermal stresses, it is sufficient to only incorporate the silicon, diamond, and GaN layers into our simulations. By implementing the effective elastic modulus from Eq. (4), a major gradient in the stress across the GaN layer was seen in each step of the simulation. This implies that stress relaxation due to TDs is present from the initial phase of the wafer, i.e., following MOCVD growth of the nitride layers. The range of experimental stress values for UV and visible micro-Raman is shown in Fig. 3 using patterned rectangles with the vertical dimension corresponding to the standard deviations from each map and the horizontal dimension representing the optical probe depth for each particular measurement. Figure 3 presents the resulting simulated σ_{xx} as a function of vertical material cross-section. The abrupt shape of this dependence is due to the simple two-region model used here. Good agreement with the measured stress is obtained using relaxation factors of $f_{GaN/D} = 0.76$ in the GaN close to the GaN/D interface and $f_{GaN} = 0.095$ near the AlGaN-GaN interface. Details of the simulations will be published separately.

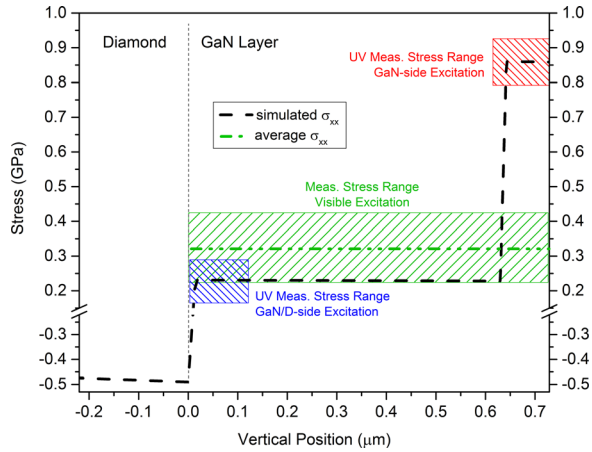

FIG. 3. Results from FE simulation of stress as a function of vertical material cross-section. The simulated stress is shown as a dashed line. The measured stress values from visible and from UV micro-Raman for each side of the wafer are represented as patterned rectangles with the vertical dimension corresponding to standard deviations and horizontal dimension the depth optically probed for each measurement.

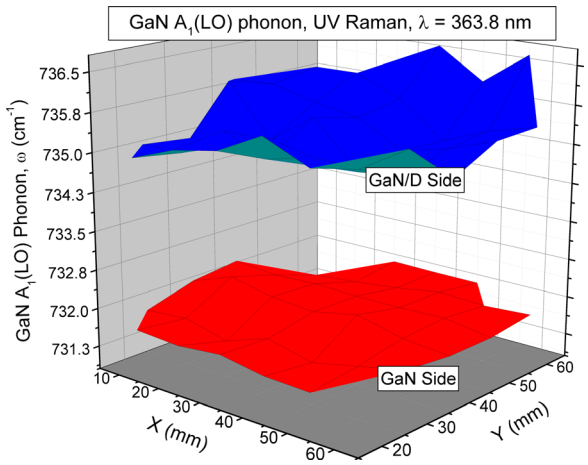

FIG. 4. Map of the A_1(LO) phonon energy using UV micro-Raman spectroscopy. The upper (lower) manifold correlates to measurements made from the GaN/D (GaN) side of the wafer.

The presence of TDs is confirmed using bright-field TEM imaging. A cross-section was prepared for TEM imaging by focused ion beam (FIB) milling. The sample was milled to electron transparency at 30 kV followed by polishing steps at 5 and 2 kV before being transferred to the TEM for imaging. A representative image from the cross-section is shown in Fig. 1(c). TDs are observed in the GaN layer with higher density on the GaN/D side. Approximate densities in both regions were accomplished by counting TDs across a cumulative TEM montage (not shown) approximately 5 μm in length. This gives estimated values of $1 \times 10^9\,\mathrm{cm}^{-2}$ and $9 \times 10^9\,\mathrm{cm}^{-2}$ for the GaN and GaN/D portions of the layer, respectively. These are in agreement with prior work for GaN grown on silicon using MOCVD.[26] Within our analysis, the ratio $f_{GaN/D}/f_{GaN} \sim 8$ should be correlated with the relative TD densities ~9. This agreement is satisfactory given that the values are obtained using very different approaches.

Using the TEM estimates of density n and the f parameters from our simulations, Eq. (3) allows us to estimate $L \sim 100$ nm corresponding to the lateral size of the relaxation region surrounding the TDs. This value is comparable to previously published $L \sim 400 \pm 300$ nm obtained via studies of the temperature-dependent tensile stress in GaN grown on 6H-SiC.[9]

Lastly, we turn our attention to observed shifts in the A_1(LO) phonon energy. The mapping results of the A_1(LO) phonon for UV Raman are shown in Fig. 4. Using the Raman-stress factor for this phonon, $k_R^{A1(LO)} = -2.14 \pm 0.28\,\mathrm{cm}^{-1}/\mathrm{GPa}$,[12] and the stress-free reference frequency $\omega_0 = 733.9 \pm 0.1\ \mathrm{cm}^{-1}$, we estimate the stress-induced shifts on the GaN and GaN/D sides of the wafer. For the GaN-side, we expect a shift of $-1.8 \pm 0.2\,\mathrm{cm}^{-1}$. The measured A_1(LO) shift is $-2.1 \pm 0.2\,\mathrm{cm}^{-1}$, where the uncertainty is the standard deviation from our map measurements. The stress-induced and measured shifts are within total uncertainty of each other. For the GaN/D side, we expect a shift of $-0.5 \pm 0.1\ \mathrm{cm}^{-1}$ due to stress alone. However, the shift observed for the GaN/D side A_1(LO) phonon is $+1.5 \pm 0.5\,\mathrm{cm}^{-1}$. This corresponds to a total discrepancy of $\sim 2\,\mathrm{cm}^{-1}$. A plausible explanation for this blue shift is the presence of free carriers due to unintentional doping during the wafer processing.[27] In the presence of free carriers, phonon-plasmon coupling will blue shift LO phonons.[28] We estimate a carrier concentration $\sim (1.88 \pm 0.79) \times 10^{17}\,\mathrm{cm}^{-3}$ in the region near the GaN-diamond interface.[28] Possible sources for this unintentional doping are diffusion from the dielectric adhesion layer, from hydrogen which is present during CVD diamond growth, or from exposure during processing steps such as removal of the nitride transition layers.[29]

To summarize, spatial mapping of stresses across a 75-mm GaN-on-diamond wafer was accomplished using visible and UV micro-Raman spectroscopy. Utilizing the shallow penetration depth of UV excitation and probing both sides of the wafer, E_2^2 phonon shifts yield average tensile stresses from the top and bottom 100–130-nm regions of the GaN buffer layer of 0.86 ± 0.07 GPa and 0.23 ± 0.06 GPa, respectively. These measurements reveal an unanticipated stress gradient between the top and bottom interfaces of the 730-nm GaN layer. FE simulations are used to incorporate the presence of threading dislocations in the GaN, with different densities in the GaN/D and GaN sides of the wafer. UV and visible micro-Raman results are well-described by the simulations with relaxation parameters as the only fit variables. UV Raman measurements of the A_1(LO) phonon suggest the presence of unintentional dopants on the GaN/D side subsequent to the multiple high-temperature processing steps that follow the GaN MOCVD growth.

Texas State University and Georgia Tech would like to acknowledge the financial support of DARPA under Dr. Linton Salmon and Dr. Avram Bar Cohen.

[1]M. Nazari, B. L. Hancock, E. L. Piner, and M. W. Holtz, IEEE Trans. Electron Devices **62**, 1467 (2015).
[2]K. D. Chabak, J. K. Gillespie, V. Miller, A. Crespo, J. Roussos, M. Trejo, D. E. Walker, G. D. Via, G. H. Jessen, J. Wasserbauer, F. Faili, D. I. Babić, D. Francis, and F. Ejeckam, IEEE Electron Device Lett. **31**, 99 (2010).
[3]J. G. Felbinger, M. V. S. Chandra, Y. Sun, L. F. Eastman, J. Wasserbauer, F. Faili, D. Babic, D. Francis, and F. Ejeckam, IEEE Electron Device Lett. **28**, 948 (2007).
[4]R. H. Zhu, J. Y. Miao, J. L. Liu, L. X. Chen, J. C. Guo, C. Y. Hua, T. Ding, H. K. Lian, and C. M. Li, Diamond Relat. Mater. **50**, 55 (2014).

[5]D. Francis, F. Faili, D. Babić, F. Ejeckam, A. Nurmikko, and H. Maris, Diamond Relat. Mater. **19**, 229 (2010).
[6]D. Francis, J. Wasserbauer, and F. Faili, in *Proceedings of the CS MANTECH*, Austin, TX (2007), p. 133.
[7]C. Kisielowski, J. Krüger, S. Ruvimov, T. Suski, J. Ager, E. Jones, Z. Liliental-Weber, M. Rubin, E. Weber, M. Bremser, and R. Davis, Phys. Rev. B **54**, 17745 (1996).
[8]S. Tripathy, S. J. Chua, P. Chen, and Z. L. Miao, J. Appl. Phys. **92**, 3503 (2002).
[9]I. Ahmad, M. Holtz, N. N. Faleev, and H. Temkin, J. Appl. Phys. **95**, 1692 (2004).
[10]M. Chu, A. D. Koehler, A. Gupta, T. Nishida, and S. E. Thompson, J. Appl. Phys. **108**, 104502 (2010).
[11]B. S. Kang, S. Kim, J. Kim, F. Ren, K. Baik, S. J. Pearton, B. P. Gila, C. R. Abernathy, C. C. Pan, G. T. Chen, J. I. Chyi, V. Chandrasekaran, M. Sheplak, T. Nishida, and S. N. G. Chu, Appl. Phys. Lett. **83**, 4845 (2003).
[12]S. Choi, E. Heller, D. Dorsey, R. Vetury, and S. Graham, J. Appl. Phys. **113**, 093510 (2013).
[13]J. Wagner, H. Obloh, M. Kunzer, M. Maier, K. Köhler, and B. Johs, J. Appl. Phys. **89**, 2779 (2001).
[14]G. D. Via, J. G. Felbinger, J. Blevins, K. Chabak, G. Jessen, J. Gillespie, R. Fitch, A. Crespo, K. Sutherlin, B. Poling, S. Tetlak, R. Gilbert, T. Cooper, R. Baranyai, J. W. Pomeroy, M. Kuball, J. J. Maurer, and A. Bar-Cohen, Phys. Status Solidi C **11**, 871 (2014).
[15]A. D. Williams and T. D. Moustakas, J. Cryst. Growth **300**, 37 (2007).
[16]H. Windischmann and G. F. Epps, J. Appl. Phys. **69**, 2231 (1991).
[17]COMSOL, Inc., 2015.
[18]C. H. Xu, C. Z. Wang, C. T. Chan, and K. M. Ho, Phys. Rev. B **43**, 5024 (1991).
[19]M. J. Edwards, C. R. Bowen, D. W. E. Allsopp, and A. C. E. Dent, J. Phys. D: Appl. Phys. **43**, 385502 (2010).
[20]C. Roder, S. Einfeldt, S. Figge, and D. Hommel, Phys. Rev. B **72**, 085218 (2005).
[21]H. Watanabe, N. Yamada, and M. Okaji, Int. J. Thermophys. **25**, 221 (2004).
[22]G. Nootz, A. Schulte, L. Chernyak, A. Osinsky, J. Jasinski, M. Benamara, and Z. Liliental-Weber, Appl. Phys. Lett. **80**, 1355 (2002).
[23]N. Faleev, H. Temkin, I. Ahmad, M. Holtz, and Y. Melnik, J. Appl. Phys. **98**, 123508 (2005).
[24]H. L. Duan, J. Wang, Z. P. Huang, and B. L. Karihaloo, J. Mech. Phys. Solids **53**, 1574 (2005).
[25]J. C. Roberts, J. W. Cook, P. Rajagopal, E. L. Piner, and K. J. Linthicum, MRS Proceedings **1068**, 1068-C06-03 (2008).
[26]A. Vescan, J. D. Brown, J. W. Johnson, R. Therrien, T. Gehrke, P. Rajagopal, J. C. Roberts, S. Singhal, W. Nagy, R. Borges, E. L. Piner, and K. Linthicum, Phys. Status Solidi C **0**, 52 (2002).
[27]M. Kuball, Surf. Interface Anal. **31**, 987 (2001).
[28]H. Harima, J. Phys.: Condens. Matter **14**, R967 (2002).
[29]D. Y. Song, A. Chandolu, N. Stojanovic, S. A. Nikishin, and M. Holtz, J. Appl. Phys. **104**, 064309 (2008).